Improved nearside gravity field of the Moon by localizing the power law constraint

Shin-Chan Han,[1,2] Erwan Mazarico,[1,3] and Frank G. Lemoine[1]

Received 8 April 2009; revised 1 May 2009; accepted 5 May 2009; published 9 June 2009.

[1] The problem associated with the large data gap on the farside of the Moon is addressed for constructing a high-resolution global gravity model. By localizing the power law constraint and making it effective only within the farside and limb regions, we mitigate the undesired power-limiting effect on the nearside. Compared to the solution estimated from Lunar Prospector and other satellite tracking data with the globally-applied power law, the locally-constrained solution shows significant improvement of the nearside gravity estimates. Around the areas dominated by craters in the southern hemisphere of the nearside, the correlation with topography approaches nearly 0.95 and the admittance converges to 100–110 mGal/km up to spherical harmonic degree 130, while the globally-constrained solutions distort starting at degree 90. The proposed analysis can benefit the science and operation of other existing and future planetary missions and enhance the geophysical interpretation of the gravity field. **Citation:** Han, S.-C., E. Mazarico, and F. G. Lemoine (2009), Improved nearside gravity field of the Moon by localizing the power law constraint, *Geophys. Res. Lett.*, *36*, L11203, doi:10.1029/2009GL038556.

1. Introduction

[2] Direct tracking of the lunar-orbiting satellites from the Earth is not possible over the farside due to the synchronous rotation of the Moon about the Earth. Only the limb region of the farside is covered but with increased measurement noise [*Konopliv et al.*, 2001], which results in a lack of direct Doppler data over ~40% of the entire lunar surface. Recently, the SELENE mission obtained 4-way Doppler data over the farside by indirectly tracking the main orbiter with a small relay satellite [*Namiki et al.*, 2009]. Those data improved the farside gravity to spherical harmonic degree ~90. However, high-resolution gravity information still comes from satellites with lower orbiting altitudes such as Lunar Prospector [*Konopliv et al.*, 2001], for which no farside tracking data are available. The orthogonal sets of spherical harmonic functions are the candidates to parameterize the Newtonian potential fields since they satisfy the Laplace differential equations. However, not all of them are necessarily resolvable especially under the circumstance that the noisy data are not available uniformly over the globe. In order to overcome such problem, the power law, or Kaula's rule [*Kaula*, 1966], has been often used to obtain solutions of the gravitational fields of the planetary bodies from analysis of un-evenly sampled tracking data.

[3] The power law constraint, although it biases the solution, stabilizes a global gravity field parameterized with (non-localized) spherical harmonic functions, up to the spatial resolution corresponding to the orbiting altitude, by preventing high-degree terms from developing excessive power [e.g., *Marsh et al.*, 1990; *Lemoine et al.*, 1997; *Smith et al.*, 1999; *Konopliv et al.*, 2001]. The exploitation of Doppler tracking data over the nearside of the Moon, however, is limited due to the farside data gap, no matter how high a gravity field is modeled in degree and order, as noted by *Konopliv et al.* [2001]. Recently, *Han* [2008] proposed that the global gravity field can be modeled by implementing an alternative set of basis functions (both regionally-concentrated ones and their complements). The advantage over the ubiquitous spherical harmonic representation is that the nearside gravity field can be estimated without introducing the power law constraint. It is then also possible to simultaneously construct the nearside gravity field to a high resolution in order to fully exploit the low altitude measurements and the farside gravity field with a low resolution.

[4] In this study, we extend the work by *Han* [2008] discussing regional gravity fields with the line-of-sight acceleration measurements, but in a fully dynamic mode, to develop optimally-constrained global gravity models of the Moon. The innovation is to apply the power law constraint only over the farside and limb regions where direct observations are non-existent or the observational constraint is weak because of tracking geometry. The nearside gravity field is estimated based on the tracking data to degree and order 150. On the contrary, the farside gravity field is obtained by means of the nearside tracking data and the power law constraint.

2. Lunar Tracking Data

[5] In preparation for the Lunar Reconnaissance Orbiter (LRO) mission, historical radio tracking data were analyzed at the NASA Goddard Space Flight Center (GSFC) [*Mazarico et al.*, 2008]. One goal was to have these data ready to be incorporated early in the mission when there would still be an insufficient number of new LRO measurements to obtain a satisfactory high-resolution and high-quality gravity field solution. We use data from the following spacecraft missions; Lunar Orbiter 4 and 5, Apollo 15 and 16 sub-satellites, Clementine and Lunar Prospector (LP). With its low-altitude (~100 km and ~50 km in the nominal and extended phases, respectively) polar orbit, LP is the main contributor to the lunar data coverage over the near-

[1]Planetary Geodynamics Laboratory, NASA Goddard Space Flight Center, Greenbelt, Maryland, USA.
[2]GEST, University of Maryland Baltimore County, Baltimore, Maryland, USA.
[3]ORAU NASA Postdoctoral Program, USA.

0094-8276/09/2009GL038556$05.00

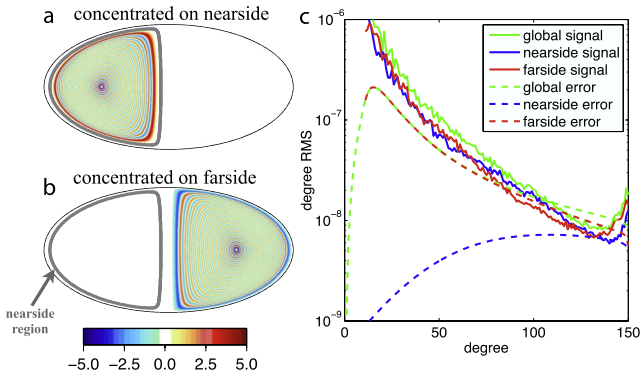

Figure 1. Examples of spherical basis functions concentrated on the (a) nearside and (b) farside. The inside of the gray cap contains the nearside area where the power law constraint may not be applied. Both functions are global-support, harmonic, orthogonal, and expanded using spherical harmonic functions to degree and order 100. The amplitude (color scale) may change depending on normalization convention. (c) Degree RMS curves of the globally-constrained gravity solution and its error estimate and of the signal and error estimates localized at the nearside and farside.

side. The radio tracking data were processed with the orbit determination software GEODYN II [*Pavlis et al.*, 2009]. Trajectory arcs up to a few days in length were integrated using force models, and various arc parameters were iteratively modified to best fit the tracking observations. The major constraints on the spacecraft orbits are range-rate (S-Band Doppler) measurements, although a significant amount of range data were collected by the Lunar Prospector mission. The partial derivatives of those measurements with respect to the spherical harmonics functions were calculated and accumulated into a set of normal equations up to degree and order 150. A first gravity solution was obtained by applying the Kaula's law such that the variance of each spherical harmonic coefficient follows $6.25 \times 10^{-8}\, l^{-4}$ [*Konopliv et al.*, 2001].

3. Localized Spherical Basis Functions

[6] For the locally-constrained solution, we first express the gravity field using alternative basis functions localized at the nearside and at the farside. Both sets of the basis functions are orthogonal and span the same vector space constructed by usual spherical harmonic basis functions [*Simons and Dahlen*, 2006]. Figures 1a and 1b show two examples of spherical, orthonormal, and localized basis functions; Figure 1a is concentrated within the nearside, and Figure 1b is concentrated within the farside. As discussed by *Han* [2008], the parameterization with respect to those localized basis functions can be done simply by a linear transformation of the spherical harmonic functions. The nearside gravity field, when parameterized with those basis functions, can be resolved even with the farside tracking data gap. However, an a priori constraint is mandatory to resolve the basis functions concentrated on

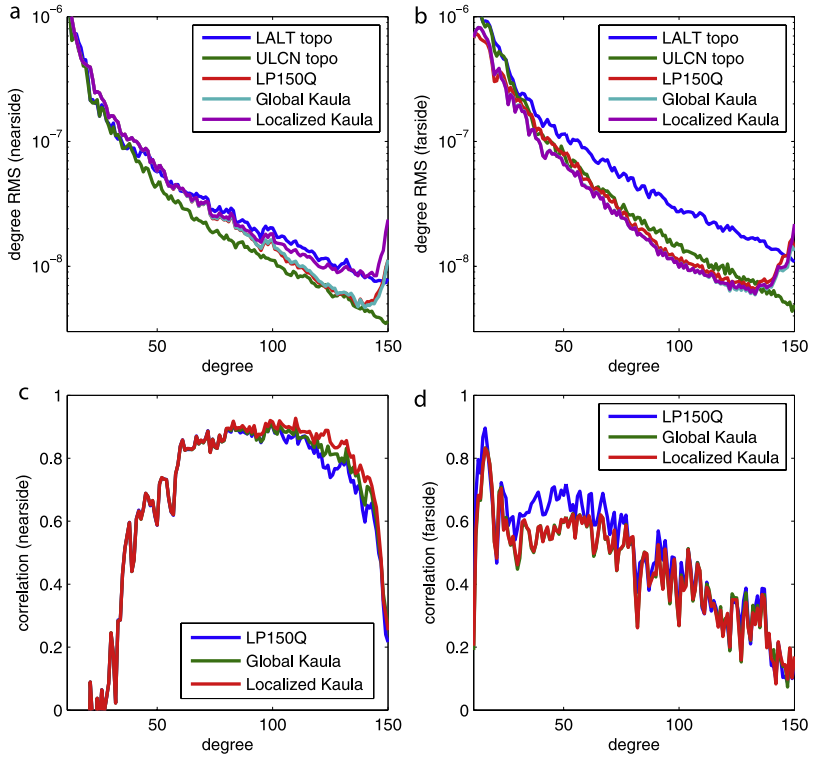

Figure 2. (top) Degree RMS of the globally-constrained solution, locally-constrained solution, LP150Q, ULCN, and LALT uncompensated topography (a) at the nearside and (b) at the farside. (bottom) Correlation of the globally-constrained solution, locally-constrained solution, and LP150Q with LALT topography (c) at the nearside and (d) at the farside.

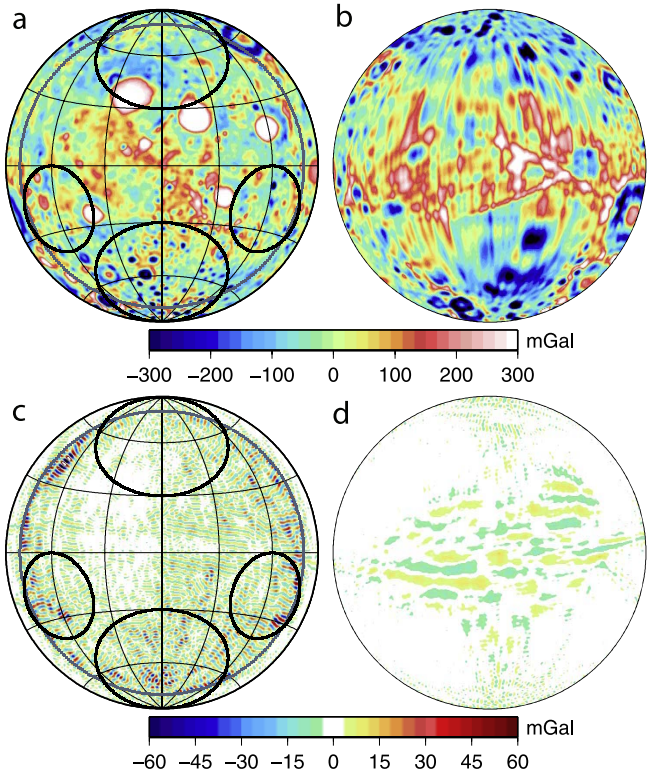

Figure 3. (top) Radial gravity, evaluated at the mean surface and truncated at degree 140, from the locally-constrained solution for (a) the nearside and (b) the farside. (bottom) Radial gravity difference between the locally-constrained and globally-constrained solutions for (c) the nearside and (d) the farside. The gray circle delineates the nearside area where the Kaula's power law constraint is not applied. The black circles show the local areas of interest in the nearside, highlighting the additional signals not diminished by the power law.

the farside. Unlike *Han* [2008], we construct the global gravity field using concentrated basis functions at the nearside (with a concentration ratio greater than 0.5) and their complements.

[7] Figure 1c shows the global gravity model estimated with various satellite tracking data as described in Section 2 by applying the Kaula's power law globally such as was done by *Lemoine et al.* [1997] and *Konopliv et al.* [2001]. The linear transformation matrix was applied to decompose the global spherical harmonic solution into the nearside and farside gravity fields separately. In addition, the full error covariance matrix of the global gravity solution was propagated to compute the error estimates of the gravity field coefficients localized over the nearside and the farside. Since the errors of the lunar gravity model are highly non-stationary, the global error estimate is heavily biased toward the farside error. However, when the error covariance matrix is localized, we can quantify the nearside gravity signal-to-noise ratio (SNR). It is larger than 10 up to degree 60, and is greater than unity up to degree 140, beyond which the signal aliasing effect causes increasing power with increasing degree. On the other hand, the farside gravity estimate is of poorer quality with SNR slightly larger than or close to unity for most degrees (except very low degrees) and no longer significant beyond degree 70 or so.

4. Global Gravity Field With the Localized Power Law Constraint

[8] For our new global gravity solution, the normal matrix calculated by integrating the equations of motion and parameterized with the spherical harmonic basis was transformed and expressed in the localized spherical basis as described in Section 3. Then we implemented the power law constraint in terms of the alternative basis functions. Only the basis functions concentrated on the farside including the limb region were constrained for the least-square solution with the same Kaula rule as previously. In contrast, the gravity field over the nearside (delineated with a spherical cap centered at 0°N and 0°E with a cap size of 80°; see the circle in Figure 1) is recovered relying on the tracking data alone. We address the improvement of the nearside gravity by comparing the locally-constrained and globally-constrained gravity solutions, LP150Q gravity [*Konopliv et al.*, 2001], ULCN topography [*Archinal et al.*, 2006], and SELENE LALT topography [*Araki et al.*, 2009].

[9] Figures 2a and 2b show the degree RMS of the gravitational potentials caused by uncompensated topography and of LP150Q, globally-constrained solution, and locally-constrained solution at the nearside and the farside. In both hemispheres, significant differences exist between LALT and ULCN topography, indicating that ULCN topography is probably too smooth. For the nearside, all three gravity models follow the LALT topography power spectrum to degree 80 or so; however, beyond such degree, LP150Q and globally-constrained solution follow the ULCN topography power spectrum by lacking power in higher degrees. Meanwhile, the locally-constrained solution follows the LALT topography power spectrum to degree 140, where the aliasing effect starts to be pronounced. Within the band from degree 90 to 130, the agreement of the power spectra between the locally-constrained solution and LALT topography is outstanding, which can be noted in how closely the curves match, even for small degree-range jumps. This shows that, when applied globally, the Kaula constraint artificially diminishes the nearside gravity information, especially at the high degrees ($l,m \geq 100$). Over the farside, all gravity solutions follow ULCN topography, significantly losing power with increasing degree. This is not surprising as all three gravity solutions had little observational contribution and were obtained by means of the power law to degree and order 150.

[10] Figures 2c and 2d present the correlation of the three gravity solutions with LALT topography. On the nearside and for the high degrees ($l,m \geq 100$), GSFC's globally-constrained solution is more correlated with topography than LP150Q (partly due to the use of LP data with higher weights), but the correlation in the locally-constrained solution is even better. However, for the low degrees ($l,m \leq 80$) and over the farside, LP150Q shows better correlation while the topography correlation of both GSFC solutions are essentially the same. The lower correlation of GSFC gravity fields over the farside could be partially due to the lack of Lunar Orbiter 1–3 data, not incorporated at this time.

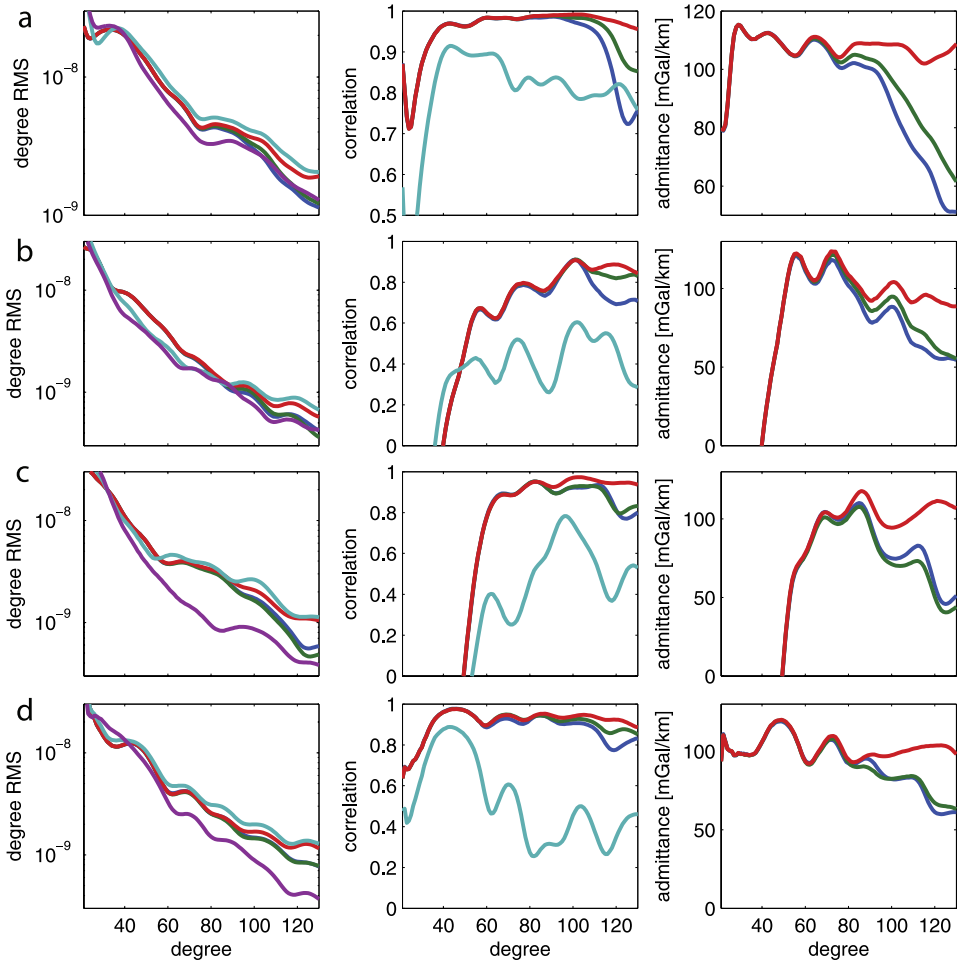

Figure 4. Degree RMS, correlation, and admittance of gravity and topography localized at various regions centered at (a) 60S/0E, (b) 60N/0E, (c) 20S/60W, and (d) 20S/60E (from Top to Bottom) marked with the black circles in Figure 3. For degree RMS, LP150Q (blue), globally-constrained solution (green), locally-constrained solution (red), uncompensated topography of ULCN (magenta) and LALT (cyan). For correlation, LP150Q and LALT (blue), globally-constrained solution and LALT (green), locally-constrained solution and LALT (red), and locally-constrained solution and ULCN (cyan). For admittance, LP150Q and LALT (blue), globally-constrained solution and LALT (green), and locally-constrained solution and LALT (red).

[11] The radial gravity component computed from the locally-constrained solution and its difference with the globally-constrained solution are shown in Figure 3, over both the nearside and farside hemispheres. It highlights the additional anomalies that were diminished by the power law in the globally-constrained solution. Because the localized basis functions have global-support to satisfy the harmonic condition on a sphere, there are small but non-zero differences, less than ~10 mGal (10^{-5} m/s^2), over the farside and at long wavelengths between the globally- and locally-constrained solutions. The unconstrained basis functions, although mostly concentrated over the nearside, still have a (minor) impact over the farside.

[12] Figure 4 shows degree RMS, topography correlation, and admittance from the three gravity solutions, localized in four individual regions of interest over the nearside (black circles in Figure 3), following *Wieczorek and Simons* [2005]. In all the regions, the locally-constrained gravity solutions, which were not affected by the power law, yield power spectra following the gravitational power spectra of the uncompensated LALT topography better than the other gravity solutions. Similarly to what was seen within the whole nearside region, when constrained by the power law, the power at higher degrees ($l,m \geq 100$) is too low. Although the Kaula power law constrains only the amplitude of each gravity coefficient, the phase of gravity coefficient is also affected when applied in the least-square inversion, which is evident from a cross correlation with topography. The locally-constrained gravity field shows improved correlation with LALT topography over the subset nearside regions, which is most notable at high degrees. The correlation of the locally-constrained solution (the most preferable solution) with ULCN topography is far below the one with LALT topography, indicating a significant improvement in the new LALT topography.

[13] The admittance spectrum is computed by multiplying the square-root of the ratio between gravity and topography power spectra to the correlation spectrum as follows:

$$\frac{\Phi_{gh}}{\Phi_{hh}} = \frac{\Phi_{gh}}{\sqrt{\Phi_{gg}\Phi_{hh}}}\sqrt{\frac{\Phi_{gg}}{\Phi_{hh}}}, \quad (1)$$

where Φ_{gg} and Φ_{hh} are the power spectrum of the gravity and topography, respectively. Φ_{gh} is the cross power spectrum between gravity and topography. $\frac{\Phi_{gh}}{\Phi_{hh}}$ and $\frac{\Phi_{gh}}{\sqrt{\Phi_{gg}\Phi_{hh}}}$ are the admittance and correlation spectrum, respectively. They are computed at each degree averaging over orders (i.e., azimuth-average). The power law constraint tends to diminish Φ_{gg} especially at higher degrees, and yields underprediction of the gravity-topography ratio, $\sqrt{\frac{\Phi_{gg}}{\Phi_{hh}}}$. However, this can be alleviated by localizing the power law only over the farside, and thus the gravity-topography power ratio can then be better estimated over the nearside. Consequently, in addition to improving the correlation, the locally-constrained gravity solution yields even further improvement in the admittance estimates.

[14] Low correlation and negative admittance appear in low degrees from all gravity solutions, due to the lunar mass concentrations [*Muller and Sjogren*, 1968]. We looked at various other nearside regions and found enhancement in degree RMS, correlation, and admittance for all the cases except the area centered around 40°N and 60°W where no significant high-frequency gravity and topography signals are expected.

5. Summary

[15] We report improvement in the global gravity solution of the Moon by implementing a power law constraint effective only within the farside and the limb region. The gravity field over the nearside is not optimally estimated with a globally-applied power law constraint, especially at high degrees. Differences of several tens of mGal were found between the locally- and globally-constrained solutions over the nearside. Most of these differences are likely to be actual signals since they reconcile the gravity solution with the power spectrum of uncompensated topographical potential and increase the correlation with topography. The admittance estimates, that are most critical to reveal the physical processes of the lunar surface and interior, are most significantly improved. We quantified the gravity signal and (highly non-stationary) error estimates over the nearside and farside, separately. A more realistic error spectrum estimate of the nearside gravity was demonstrated by performing a full error covariance propagation, as also discussed by *Floberghagen et al.* [1999]. Although the areas to be constrained by the power law should be optimized considering the intrinsic signal strength, tracking data coverage, and data noise, the new technique demonstrated in this study shows promising results by better exploiting the nearside observations for the global gravity analysis. This study can easily be extended to process the data from other lunar missions such LRO, and other planet-orbiting satellite missions such as Mars Reconnaissance Orbiter (for instance, to improve the gravity field over Tharsis). It could be beneficial for the Mercury gravity field, because the MESSENGER spacecraft will be in a very elliptical orbit, much closer to the planet and thus more sensitive to short-wavelength gravity anomalies over the Northern hemisphere.

[16] **Acknowledgments.** This work was supported by NASA's programs in Lunar Advanced Science and Exploration Research, Mars Data Analysis, Earth Surface and Interior, and GRACE projects. EM was supported by the NASA postdoctoral program. David Rowlands is acknowledged for his help on satellite tracking data analysis and useful discussion. Some FORTRAN codes written by Mark Wieczorek were used.

References

Araki, H., et al. (2009), Lunar global shape and polar topography derived from Kaguya-LALT laser altimetry, *Science*, *323*, 897–900.

Archinal, B. A., M. R. Rosiek, R. L. Kirk, and B. L. Redding (2006), The unified lunar control network 2005, *U.S. Geo. Surv. Open File Rep., 2006–1367*.

Floberghagen, R., J. Bouman, R. Koop, and P. Visser (1999), On the information contents and regularisation of lunar gravity field solutions, *Adv. Space Res.*, *23*, 1801–1807.

Han, S.-C. (2008), Improved regional gravity fields on the Moon from Lunar Prospector tracking data by means of localized spherical harmonic functions, *J. Geophys. Res.*, *113*, E11012, doi:10.1029/2008JE003166.

Kaula, W. M. (1966), *Theory of Satellite Geodesy*, Blaisdell, Waltham, Mass.

Konopliv, A. S., S. W. Asmar, E. Carranza, W. L. Sjogren, and D. N. Yuan (2001), Recent gravity models as a result of the Lunar Prospector Mission, *Icarus*, *150*, 1–18.

Lemoine, F. G. R., D. E. Smith, M. T. Zuber, G. A. Neumann, and D. D. Rowlands (1997), A 70th degree lunar gravity model (GLGM-2) from Clementine and other tracking data, *J. Geophys. Res.*, *102*, 16,339–16,359.

Marsh, J. G., et al. (1990), The GEM-T2 gravitational model, *J. Geophys. Res.*, *95*, 22,043–22,071.

Mazarico, E., F. G. Lemoine, G. A. Neumann, D. E. Smith, D. D. Rowlands, and M. T. Zuber (2008), Preparations for Lunar Reconnaissance Orbiter gravity and altimetry missions, *Eos Trans. AGU*, *89*(53), Fall Meet. Suppl., Abstract P31B-1401.

Muller, P. M., and W. L. Sjogren (1968), Mascons: Lunar mass concentrations, *Science*, *161*, 680–684.

Namiki, N., et al. (2009), Farside gravity field of the Moon from four-way Doppler measurements of SELENE (Kaguya), *Science*, *323*, 900–905.

Pavlis, D. E., S. Poulose, and J. J. McCarthy (2009), GEODYN operations manuals, contractor report, SGT Inc., Greenbelt, Md.

Simons, F. J., and F. A. Dahlen (2006), Spherical Slepian functions and the polar gap in geodesy, *Geophys. J. Int.*, *166*, 1039–1061.

Smith, D. E., et al. (1999), The gravity field of Mars: Results from Mars Global Surveyor, *Science*, *286*, 94–97.

Wieczorek, M. A., and F. J. Simons (2005), Localized spectral analysis on the sphere, *Geophys. J. Int.*, *162*, 655–675.

S.-C. Han, F. G. Lemoine, and E. Mazarico, Planetary Geodynamics Laboratory, NASA Goddard Space Flight Center, Code 698, Greenbelt, MD 20771, USA. (shin-chan.han@nasa.gov)